Building the Kitagawa-Takahashi diagram of flawed materials and components using an optimized V-notched cylindrical specimen

M. Benedetti[1*], C. Santus[2]

[1]Department of Industrial Engineering, University of Trento, Trento, Italy

[2]Department of Civil and Industrial Engineering, University of Pisa, Pisa, Italy

*Contacting Author:

Matteo Benedetti

Tel. +390461282457

Fax +390461281977

E-mail: matteo.benedetti@unitn.it

Abstract

The present technical note illustrates a novel procedure for building the Kitagawa-Takahashi diagram of a flawed material and of notched components made of the same material. The novelty of the method over the existing technical literature is the use of a rounded V-notched cylindrical specimen, whose geometry was optimized to maximize the intensity of the asymptotical notch stress term. In this way, the sensitivity to experimental uncertainties is reduced and no cumbersome fracture mechanics tests are requested to determine the crack threshold of the defect free of the defect-free material counterpart. The only experimental input are the high-cycle fatigue strength and the mean size of the critical defect at the notch tip of three specimen batches differing in the size of the critical defect and/or in the notch root radius. The potentiality of the method is checked for an additively manufactured Ti-6Al-4V alloy.

Keywords

Defects; Kitagawa-Takahashi diagram; Short crack effect; Additive Manufacturing; Ti-6Al-4V ELI

Nomenclature

a	Crack length
A	Notch depth (see Fig. 2)
AM	Additive manufacturing
$Area$	Area obtained by projecting a defect or a crack onto the plane perpendicular to the maximum tensile stress
$Area_{max}$	Critical defect size

a_0	El-Haddad fictitious intrinsic crack length
D	Specimen outer diameter (see Fig. 2)
HV	Vickers hardness
f_N	Correction factor of the net stress range to obtain the average stress range
LEFM	Linear elastic fracture mechanics
N_f	Number of cycles to failure
r_{eq}	Equivalent radius of the defect (Eq. (7))
R	Notch root radius
R	Load ratio
SED	Strain energy density
SIF	Stress intensity factor
SLM	Selective laser melting
TCD	Theory of critical distances
α	Notch aperture angle (Fig. 2)
β, δ	Coefficients of Eq. (14) expressing the influence of HV on σ_W
ΔK_{th}	Long-crack threshold stress intensity factor range
ΔK_{eff}	Stress intensity factor range corrected for the short crack effect and the notch stress field
ΔK_{corr}	Stress intensity factor range corrected for the short crack effect
$\Delta\sigma^\infty$	Far-field stress range
$\overline{\Delta\sigma}$	Stress range averaged over the equivalent defect size (Eq. (10))
$\Delta\sigma_{eff}$	Effective principal stress amplitude (Eq. (9))
$\Delta\sigma_{eff,th}$	Threshold effective stress range (Eq. (11))
$\Delta\sigma_0$	Defect-free material fatigue limit (stress range)
$\Delta\sigma_N$	Net nominal stress range (see Fig. 2)
σ_W	Fully-reversed high-cycle fatigue strength amplitude (Eq. (14))

1. Introduction

Defects, such as surface scratches and roughness, non-metallic inclusions, pores, foreign object damages, play a crucial role in fatigue crack initiation and propagation, thus affecting the structural integrity of cyclically loaded components in terms of lifetime and fatigue strength. To this regard, fundamental investigations [1,2] were carried out since the 70s of the last century on conventionally manufactured materials, like tool steels [3], cast Al-Si eutectic alloys [4], nodular cast iron [5], welded joints [6] and railways axles [7], as it was recognized that defects are the preferential fracture origin in such inherently flawed materials. Nowadays, the interest in incorporating the effect of defects into the fatigue design has further increased with the advent of additive manufacturing (AM) technologies, which, on one side, permit larger design freedom, on the other one, introduce into the component defects in the form of surface roughness, pores and lack of fusion [8-10].

This scenario is further complicated by the fact that, very often, machine parts are not only weakened by defects but also by geometrical details (holes, grooves, key seats, etc.), in general regarded as "notches". They perturb the lines of force flow resulting in local stress concentration that may promote the onset of fatigue damage. How to deal with the concomitant effect of defects at the microscopic level and of notches at the macroscopic one is however not straightforward. According to a global approach to the problem, one may think of the defected material as a homogenous medium with reduced fatigue properties. Its fatigue calculation can be performed by applying traditional notch fatigue methods codified in machine design manuals and based on correction coefficients accounting for the geometrical stress concentration factor and the material's notch sensitivity [11]. The low value of the plain fatigue strength, as a consequence of the inherent material defectiveness, generally results in low notch sensitivity [12]. If the notch fatigue is reinterpreted by the light of more sophisticated methods, such as the Theory of Critical Distances (TCD) [13] or based on the Strain Energy Density (SED) [14], the low material's notch sensitivity can be explained by invoking the large value of the critical distance or the control radius of the material. However, these material characteristics turn out to be defect-dependent, therefore, a specific testing campaign is necessary to calibrate their value according to the defectiveness actually present in the vicinity of the notch [15,16].

On the contrary, a local approach, which is the focus of the present technical note and will be better discussed in the following section, regards the defects as pre-existing cracks. Within the validity field of the linear-elastic fracture mechanics (LEFM), these do not propagate as long as their stress intensity factor (SIF) range ΔK_I is below the fatigue threshold ΔK_{th}. For a crack-like defect of size *2a* embedded in an infinite plate, this condition is expressed as:

$$\Delta K_I < \Delta K_{th} \tag{1}$$

$$\Delta K_I = \Delta\sigma^\infty \sqrt{\pi a}$$

Where $\Delta\sigma^\infty$ is the far-field stress range.

The Kitagawa-Takahashi diagram [17], schematically shown in Fig. 1, is a powerful tool for encapsulating fracture mechanics and stress-based approaches in the fatigue design of components: the part is regarded to be fail-safe when the applied stress range $\Delta\sigma^\infty$ is below the defect-free material fatigue limit $\Delta\sigma_0$ and when the above condition of non-propagating crack or crack-like defect is satisfied. The transition between these two failure mechanisms occurs at the crack size a_0, usually denoted as El-Haddad fictitious intrinsic crack length [18]:

$$a_0 = \frac{1}{\pi}\left(\frac{\Delta K_{th}}{\Delta\sigma_0}\right)^2 \tag{2}$$

Numerous experimental evidences attest however that small cracks can propagate at applied stress intensities less than the threshold ΔK_{th}. El Haddad, Topper and Smith [18,19] suggested that the differences in the fracture mechanics-based growth characterization for long and short cracks vanish when a_0 is added to the fatigue crack length a. Accordingly, Eq. (1) can be reformulated as follows:

$$\Delta K_{corr} < \Delta K_{th} \tag{3}$$

$$\Delta K_{corr} = \Delta\sigma^\infty \sqrt{\pi(a + a_0)}$$

The condition expressed by Eq. (3) is qualitatively indicated in Fig. 1 by the solid line.

From the above discussion, it is clear that a reliable identification of the safe in-service conditions necessitates an accurate estimation of $\Delta\sigma_0$ and ΔK_{th}, whence a_0 can be deduced. The experimental determination of ΔK_{th} is however not an easy task, as it requires sophisticated laboratory equipment and hands-on expertise, the experiments are difficult especially under negative load ratios R, the results are strongly affected by the load shedding strategy adopted during precracking [20]. In addition, in the case of flawed materials, this scenario is further complicated since it is not obvious how to determine $\Delta\sigma_0$ and ΔK_{th} of the defect-free material counterpart. Finally, if the fatigue damage triggering crack-like defect is situated in the vicinity of a notch, Eq. (3) must be modified in order to account for the deviation of the local stress from $\Delta\sigma^\infty$.

The present work is aimed at devising an alternative and indirect procedure for building the Kitagawa-Takahashi diagram of a flawed material and of notched components made of the same material, without requiring the knowledge of $\Delta\sigma_0$ and ΔK_{th} of the defect-free material counterpart. This is based on an optimized geometry of a rounded V-notched cylindrical specimen, schematically illustrated in Fig. 2, wherein the notch depth is devised to maximize the intensity of the singular stress term. This specimen geometry was originally employed for the inverse determination of the TCD critical distance [21] and the SED control radius [16]. In this work, the same specimen geometry is used to identify the propagation condition of crack-like defects. The only experimental input are the high-cycle fatigue strength and the mean size of the critical defect at the notch tip. Section 2 provides the theoretical background of this procedure, while in Section 3 the proposed method is applied to build the Kitagawa-Takahashi diagram of Ti-6Al-4V additively manufactured via Selective Laser Melting (SLM). The conclusions close the technical note.

2. Theoretical background

Equations (1) and (3) hold true for a crack centered in an infinitely wide plate; therefore, a shape factor γ must be introduced for the sake of generality:

$$\Delta K_{corr} = \Delta\sigma^\infty \sqrt{\pi(\gamma^2 \cdot a + a_0)} \tag{4}$$

In his pioneering works, Murakami [22] showed that the SIF of a defect is related to the $\sqrt{area}$ parameter, defined as the square root of the area obtained by projecting a defect or a crack onto the plane perpendicular to the maximum tensile stress. More specifically, the maximum value of K_I along the boundary of a surface or sub-surface crack-like defect can be approximated as:

$$K_I = 0.65 \cdot \sigma^\infty \sqrt{\pi\sqrt{area}} \tag{5}$$

In their illuminating paper, which gave inspiration to the present work, Meneghetti et al. [23] proposed the following expression of Eq. (4) to preserve the SIF equality with respect to Eq. (5):

$$\Delta K_{corr} = \Delta\sigma^\infty \sqrt{\pi(0.65^2 \cdot \sqrt{area} + a_0)} \tag{6}$$

Importantly, Eq. (5) was derived by Murakami for a crack of arbitrary shape in a uniformly stressed infinite plate. In a first simplified attempt to the problem of a defect located in the vicinity of a stress raiser (see Fig. 2), we propose to modify Eq. (6) by replacing the far-field stress σ^∞ with the normal principal stress $\bar{\sigma}$

averaged over the defect size. Assuming for simplicity a defect of approximately circular shape, the equivalent radius r_{eq} of the defect is related to its area through the following expression:

$$r_{eq} = \sqrt{\frac{area}{\pi}} \tag{7}$$

As shown by Tada [24], this hypothesis is reasonable inasmuch the defect size $2r_{eq}$ is much lower than the notch depth A ($2r_{eq}/A \leq 0.1$). Based on the above considerations, the SIF range of a crack-like defect will be then corrected for both the short crack effect and the notch stress field according to the following expression:

$$\Delta K_{eff} = \Delta\sigma_{eff}\sqrt{\pi\left(0.65^2 \cdot \sqrt{area} + a_0\right)} \tag{8}$$

Where the effective stress range $\Delta\sigma_{eff}$ is related to either $\Delta\sigma^\infty$ or the notch stress field averaged over the crack length $\overline{\Delta\sigma}$ according to the following expression:

$$\Delta\sigma_{eff} = \begin{cases} \Delta\sigma^\infty & no\ stress\ concentration\ (plain) \\ \overline{\Delta\sigma} & notch \end{cases} \tag{9}$$

As schematically shown in Fig. 2, the average stress range $\overline{\Delta\sigma}$ can be calculated as:

$$\overline{\Delta\sigma} = \frac{1}{2r_{eq}}\int_0^{2r_{eq}} \Delta\sigma_y\, dx = f_N\Delta\sigma_N \tag{10}$$

and expressed as a function of the notch net nominal stress range $\Delta\sigma_N$. It is worth noticing that the coefficient $f_N = \overline{\Delta\sigma}/\Delta\sigma_N$ can be thought of as the fatigue stress concentration factor K_f estimated according to the Line Method of TCD, wherein the critical length $L = r_{eq}$ [13]. A specific advantage of the proposed method is that the user is not requested to perform any FEM calculation of the notch stress field, as analytical formulas were derived in [21] to express K_f (and hence f_N) as a function of the notch opening angle α and the dimensionless notch root radius $\frac{R}{D/2}$. A MATLAB® function for the estimation of f_N is provided in the online version of the present article. The use of this script is briefly explained in Appendix A.

By imposing the failure condition $\Delta K_{eff} = \Delta K_{th}$, the threshold effective stress range can be readily determined as:

$$\Delta\sigma_{eff,th} = \frac{\Delta K_{th}}{\sqrt{\pi\left(0.65^2 \cdot \sqrt{area}_{max} + a_0\right)}} \tag{11}$$

The unknown parameters a_0 and ΔK_{th} can be back-calculated from Eq. (11) if at least two fatigue data are known along with the corresponding $\sqrt{area}_{max}$ parameter of the (largest) critical defect. In the following applicative example, we will consider the high-cycle fatigue strength estimated from SN curves with 50% failure probability and the average $\sqrt{area}_{max}$ estimated from fractographic inspections. In particular, the inverse procedure is made more robust by least-square fitting the available experimental data, that is by minimizing the following weighted sum of square residuals:

$$WSSE = \sum_{i=1}^{n}\left(\frac{\Delta\sigma_{eff,i} - \Delta\sigma_{exp,i}}{S_i}\right)^2 \tag{12}$$

Where $\Delta\sigma_{exp,i}$ is the i-th experimental value of the effective stress range and S_i its standard deviation, and n is the number of data (at least 3 in the present case). It should be noted that the intent of this fitting procedure is to estimate the material properties with the maximum likelihood. Clearly, the use of the devised method for a

probabilistic fatigue assessment shall require the estimation of the statistical distribution of the inferred material properties.

3. An applicative example

The experimental data derived from our previous papers [15] and [25] are reconsidered in this work and analyzed with the proposed procedure. In [25], plain samples were additively manufactured by selective laser melting (SLM) of titanium alloy Ti-6Al-4V ELI and fatigue tested at the load ratio R= –1 exploring fatigue lives up to 5×10^7 cycles. In [15], notched samples with the same geometry shown in Fig. 2 (outer diameter D = 7.7 mm, α = 90°) were fabricated via SLM and fatigue-tested in the same way. To explore the effect of the defectiveness on the notch fatigue strength, two sample batches were produced. The first one, termed T-N, is obtained by turning the notch from plain cylindrical bars, while in the second batch, termed SLM-N, the notch geometry is already introduced by the SLM process and a slight turning finish was applied to restore the correct notch radius. To explore different notch severities, the specimens were provided with two distinct values of the notch root fillet radius R. Specifically, the notches with R = 0.2 mm (theoretical principal stress concentration factor K_t = 3.83) and with R = 1 mm (K_t = 1.97) will be referred to as sharp and blunt, respectively.

The SN curves of all the experimental variants are shown in Fig. 3 and are fitted using the following asymptotic function:

$$\sigma_a = c_1 + \frac{c_2}{N_f^m} \tag{13}$$

Where σ_a represents the gross (plain) and the net-nominal (notched samples) stress amplitude at the fatigue life N_f. The best-fit coefficients are listed in Table 1.

The fracture surface of 3 fatigue coupons per each experimental variant were observed by means of Scanning Electron Microscope (SEM), in order to identify the crack initiation site and to evaluate the area of the critical defect that triggered the fatigue failure. Representative SEM micrographs of critical defects found in plain, T-N and SLM-N samples are given in Fig. 4a, b, c, respectively. The results of the defect size measurements are listed in Table 2. We included in this analysis only defects found in failed samples tested at a stress amplitude not more than 15% higher than that corresponding to a fatigue life of 5×10^7 cycles, thus representative of the high-cycle-fatigue regime explored in the present work. We are aware of the low number of observed coupons, caused by the limited availability of experimental material, nevertheless we believe that the aim of the present technical note is rather to explore a new method for building the Kitagawa-Takahashi diagram. Clearly, its usage for a sound reliability assessment necessitates the analysis of a larger population of critical defects.

Looking at Table 2, it can be noted that $\sqrt{area}_{max}$ is systematically larger in the T-N than in the SLM-N specimens, while the smooth samples display an intermediate value. Interestingly, the average critical defect size found in this last condition is in very good agreement with the value (150 μm) found in [25] by applying the statistics of largest extreme value distribution [26] to the population of defects detected through the CT scan of a plain sample by considering to a cumulative probability of 99.9%. Furthermore, SEM analyses

pointed out that critical defects were located in the interior of the plain samples, whereas the killer defects were systematically found very close to the notch tip in the notched variants. The reader is referred to [15] for further detail.

In the following, we will explore the applicability of the inverse determination procedure described in Section 2, by envisaging the four scenarios listed in Table 3. In each scenario (abbreviated as "S"), three experimental datasets corresponding to a fatigue life of 5×10^7 cycles are considered, whereas the remaining two are used as an independent validation of the method. For each dataset, the average size of the critical defect is used to compute Eq. (11). Beside using plain samples, S1 (S4) employs two identical sharp (blunt) notches, differing however in the population of critical defects ahead of the notch tip. If this condition is difficult to achieve, for instance because of the impossibility of controlling the size of critical defects, either S2 or S3 may be adopted, wherein two of three datasets are based on the same population of critical defects and obtained from notched samples of different geometry.

Table 4 lists the estimation of the two model parameters a_0 and ΔK_{th} along with $\Delta \sigma_0$ determined from Eq. (2) for the four scenarios. Interestingly, the agreement among the estimations of the four scenarios is fairly good, also in view of the large uncertainty of the experimental data. The estimates of the fatigue threshold ΔK_{th} are comprised between 7.3 and 7.5 MPa m$^{0.5}$, while fatigue crack growth tests undertaken in [15] on the same material resulted in ΔK_{th} of about 3.7 MPa m$^{0.5}$. Interestingly, an estimation of ΔK_{th} comprised between 4.5 and 5.5 MPa m$^{0.5}$ (thus in better agreement with the experimental value) is obtained when replacing in Eq. (12) the material fatigue properties corresponding to 99.7% survival probability (wherein $\sigma_{a,P99.7} = \sigma_{a,P50} - 3S$). The fictitious crack length a_0 is in fairly good agreement (particularly for S1) with the value 0.012 mm indicated in [27] for Ti-6Al-4V under the same load ratio. Moreover, the estimates (especially S1-3) of the defect-free fatigue limit $\Delta \sigma_0/2$ are in good agreement with the value of 457 MPa indicated in [28] for conventionally processed Ti-6Al-4V under R=–1. Anyway, such estimations (particularly S4) are well below the value of 610 MPa estimated according to the formula $\Delta \sigma_0/2 = 1.6 \times HV$ [28] (here HV=382) that excludes any influence of defects on the material plain fatigue limit. It is worth noticing that the above comparisons with the existing literature are difficult because of the variety of microstructural conditions and defectiveness displayed by Ti-6Al-4V [29]. A direct defect tolerance assessment of the material through the present approach may be a viable solution to make up for the lack of information about these material properties.

Table 5 reports the predictions of the fatigue strength of all the investigated experimental variants for S1-4. The prediction error is satisfactory, being the maximum absolute error about 17%, that is slightly higher than that reported in [15,16] for the calculations obtained applying the global approaches based on TCD (8%) and SED (5%). On the other hand, a notable advantage of the present local approach is that it is independent of the material defectiveness, whereas the aforementioned global approaches, unless interpolation at intermediate defect size (refer to [15] for further detail), require a specific calibration for each critical defect size.

Interestingly, the lowest value of the r.m.s. error is obtained when calibrating the parameters according to scenarios 2 and 3, employing notched samples of different notch severity yet with similar defectiveness. Apparently, it is preferable to tune the present model under different stress gradients ahead of the notch tip.

To conclude, it is now possible to build the Kitagawa-Takahashi diagram by recourse to the optimal parameters listed in Table 4. For the sake of brevity, this is only plotted for the best two scenarios, viz. S2 (Fig. 5a) and S3 (Fig. 5b). Beside the threshold stress amplitude for crack propagation (Eq. (11)), Fig. 5 reports also the effective stress amplitude calculated for the 15 (plain and notched) specimens that were fatigue-fractured and then examined by SEM to get the size of the dominant defect. It can be noted that, in both cases, Eq. (11) in combination with the optimal parameters determined according to S2 and S3 is consistent with the experimental data, even with those obtained with samples not used for estimating the model parameters. The fact that the experimental data corresponding to tests that ended with the sample failure fail outside the safe region and that most of the experimental data obtained at long fatigue life ($N_f \geq 2 \times 10^6$ cycles) are closer to the boundary of the safe region than the other ones ($N_f < 2 \times 10^6$ cycles) proves the soundness of the proposed method.

In addition, Fig. 5 plots also the expression proposed by Murakami [29] to estimate the high-cycle fatigue strength σ_W (stress amplitude at R=–1) of a material of hardness HV carrying a defect of size $\sqrt{area}_{max}$:

$$\sigma_W = F_{loc} \frac{\beta \cdot HV + \delta}{\left(\sqrt{area}_{max}\right)^{1/6}} \tag{14}$$

Where F_{loc} depends upon the defect location and is equal to 1.56 for internal defects. In its original formulation, Murakami incorporated the influence of the material Vickers hardness HV in the form of a linear expression where the coefficients β and δ are equal to 1 and 120, respectively. In [25], we found that in this form Eq. (14) tends to overestimate the fatigue strength of the present Ti-alloy fabricated via SLM and proposed the following value of such coefficients, viz. $\beta = 0.83$, $\delta = 6.1$, on the base of the fatigue data obtained at two different microstructural conditions with different HV. As expected, Eq. (14) overestimates the fatigue strength of the defected material/component when used in its original formulation, whereas Eq. (14) in combination with the parameters set in [25] yields conservative estimations of the fatigue strength of the material/component (even because it implicitly assumes full notch sensitivity when applied to the results of the notched variants), apart from the experimental data relating to the sample with the largest defect. On the contrary, the criticality of this last data is properly rationalized by the fracture mechanics approach proposed in this technical note.

To conclude, we believe that these encouraging results confirm the applicability of the proposed method, which can pave the way for more sophisticated approaches able to account more accurately for the effect of defect shape, defect location and stress gradient on the SIF. Another hint for future research is the development of a probabilistic approach for defining the expected dominant defect size as a function of the distance from critical stress raisers that affect the fatigue response of machine elements. This aspect was neglected in the present work since the dominant defect was always found in the immediate vicinity of the notch tip, but in real machine elements of much larger size the interaction between notch and critical defect might be more complicated.

4. Conclusions

The following are the key conclusions that can be drawn from the present technical note:

1) The Kitagawa-Takahashi diagram of a material/component carrying defects can be deduced from the SN curve and the mean size of the critical defect of three sample batches, two of them provided with an optimized V-notched geometry.

2) The method seems to be more robust when it employs two notched variants with different notch severity.

3) In contrast to global approaches, that here proposed has the advantage of being independent of the size of the critical defect, but at the cost of slightly lower accuracy.

4) It is preferable to determine the fatigue properties of additively manufactured material/components through dedicated testing campaign rather than making use of relations derived in the past for conventionally processed materials and based on the Vickers hardness HV.

Appendix A – Software implementation

The proposed analytical procedure is available in the online page of this article, implemented in MATLAB® software. The script *Coefficients_RunFirst.m* initially needs to be run in order to have all the coefficients introduced in the Workspace and saved in the file *Coeffs.mat*.

In order to provide an example, a single calculation of the correction factor f_N can be then performed with *Example_sqrtarea2corrfact.m*, following the approach of the direct problem presented in [21].

The input data for this example, as reported in the (editable) script, is:

$\alpha = 90°$, $D = 20$ mm, $R = 0.2$ mm

$\sqrt{area} = 0.1$ mm

and the obtained result is:

$r_{eq} = 0.0564$ mm

$f_N = 3.7843$

References

[1] Usami S, Shida S. Elastic-plastic analysis of the fatigue limit for a material with small flaws. Fatigue of Engineering Materials and Structures, 1979;1:471-481.

[2] Murakami Y, Endo M. Effects of hardness and crack geometries on ΔK_{th} of small cracks emanating from small defects. In "The behaviour of short fatigue cracks", Editors K. J. Miller and E. R. de los Rios, London: M.E.P. Institution of Mechanical Engineers, 1986, pp. 275-293.

[3] Murakami Y, Endo M. Effect of defects, inclusions and inhomogeneities on fatigue strength. Int J Fatigue 1994;16:163-182.

[4] Serrano-Munoz I, Buffiere J-Y, Verdu C, Gaillard Y, Mu P, Nadot Y. Influence of surface and internal casting defects on the fatigue behaviour of A357-T6 cast aluminium alloy. Int J Fatigue 2016;82:361-370.

[5] Mu P, Nadot Y, Mendez J, Ranganathan N. Influence of casting defects on the fatigue limit of nodular cast iron. Int J Fatigue 2004;26(3):311-319.

[6]   Wu SC, Song Z, Kang GZ, Hu YN, Fu YN. The Kitagawa-Takahashi fatigue diagram to hybrid welded AA7050 joints via synchrotron X-ray tomography. Int J Fatigue 2019;125:210-221.

[7]   Wu SC, Xu ZW, Kang GZ, He WF. Probabilistic fatigue assessment for high-speed railway axles due to foreign object damages. Int J Fatigue 2018;117:90-100.

[8]   Romano S, Brückner-Foit A, Brandão A, Gumpinger J, Ghidini T, Beretta S. Fatigue properties of AlSi10Mg obtained by additive manufacturing: defect-based modelling and prediction of fatigue strength. Eng Fract Mech 2017;187:165–89.

[9]   Masuo H, Tanaka Y, Morokoshi S, Yagura H, Uchida T, Yamamoto Y, Murakami Y. Influence of defects, surface roughness and HIP on the fatigue strength of Ti-6Al-4V manufactured by additive manufacturing. Int J Fatigue 2018;117:163-179.

[10]   Carlton HD, Haboub A, Gallegos GF, Parkinson DY, MacDowell AA. Damage evolution and failure mechanisms in additively manufactured stainless steel. Mater Sci Eng A 2016;651:406–14.

[11]   Budynas RG, Nisbett JK. Shigley's mechanical engineering design. 10th ed. McGraw-Hill Education; 2014.

[12]   Taylor D, Hughes M, Allen D. Notch fatigue behaviour in cast irons explained using a fracture mechanics approach. Int J Fatigue 1996;18(7):439-445.

[13]   Taylor D. The theory of critical distances: a new perspective in fracture mechanics. Elsevier Science; 2007.

[14]   Berto F, Razavi SMJ, Torgersen J. Frontiers of fracture and fatigue: some recent applications of the local strain energy density. Frattura ed Integrita Strutturale 2018;12(43):1–32.

[15]   Benedetti M, Santus C. Notch fatigue and crack growth resistance of Ti-6Al-4V ELI additively manufactured via selective laser melting: a critical distance approach to defect sensitivity. Int J Fatigue 2019;121:281–92.

[16]   Benedetti M, Santus C, Berto F. Inverse determination of the fatigue Strain Energy Density control radius for conventionally and additively manufactured rounded V-notches. Int J Fatigue 2019;126:306-318.

[17]   Kitagawa H, Takahashi S. Applicability of fracture mechanics to very small cracks or the cracks in the early stage. In Proceedings of Second International Conference on Mechanical Behaviour of Materials, Metals Park: American Society for Metals, 1976, pp. 627-631.

[18]   El Haddad MH, Smith KN, Topper TH. Fatigue crack propagation of short cracks. J Eng Mater Technol 1979;101:42.

[19]   El Haddad MH, Topper TH, Smith KN. Prediction of non propagating cracks. Eng Fract Mech 1979;11:573–84.

[20]   Newman JC, Yamada Y. Compression precracking methods to generate near-threshold fatigue-crack-growth-rate data. Int J Fatigue, 32(6) (2010), pp. 879-885.

[21]   Santus C, Taylor D, Benedetti M. Determination of the fatigue critical distance according to the Line and the Point Methods with rounded V-notched specimen. Int J Fatigue 2018;106:208–18.

[22] Murakami Y. Analysis of stress intensity factors of modes I, II and III for inclined surface cracks of arbitrary shape. Eng Fract Mech 1985;22:101–14.

[23] Meneghetti G, Rigon D, Gennari C. An analysis of defects influence on axial fatigue strength of maraging steel specimens produced by additive manufacturing. Int J Fatigue 2019;118:54-64.

[24] Tada H, Paris PC, Irwin GR. The Stress Analysis Handbook, 2nd edn. Paris Production Inc., St. Louis (1985).

[25] Benedetti M, Fontanari V, Bandini M, Zanini F, Carmignato S. Low- and high-cycle fatigue resistance of Ti-6Al-4V ELI additively manufactured via selective laser melting: mean stress and defect sensitivity. Int J Fatigue 2018;107:96–109.

[26] Beretta S, Murakami Y. Statistical analysis of defects for fatigue strength prediction and quality control of materials. Fatigue Fract Eng Mater Struct 1998;21:1049–65.

[27] Ogawa T, Tokaji K, Ohya K. The effect of microstructure and fracture surface roughness on fatigue crack propagation in a Ti–6A1–4V alloy. Fatigue Fract Eng Mater Struct 1993;16(9):973–82.

[28] Boller C, Seeger T. Materials data for cyclic loading. Mater Sci Monogr, vol. 42E. Elsevier; 1987. Part D: Aluminium and titanium alloys.

[29] Murakami Y. Metal fatigue: effects of small defects and nonmetallic inclusions. Elsevier; 2002.

[30] Benedetti M, Fontanari V. The effect of bi-modal and lamellar microstructures of Ti-6Al-4V on the behaviour of fatigue cracks emanating from edge-notches. Fatigue Fract. Eng. Mater Struct. 2004;27: 1073–1089.

[31] Santus C, Taylor D, Benedetti M. Experimental determination and sensitivity analysis of the fatigue critical distance obtained with rounded V-notched specimens. Int J Fatigue 2018;113:113–25.

Tables

Table 1: Principal results of the fatigue tests.

Specimen geometry	c_1 (MPa)	c_2	m	$\sigma_a @ N_f = 5 \cdot 10^7$ (MPa)	S (MPa)
Plain	221	123927	0.646	225.0	24.2
Sharp turned-notch (T-N)	72	496	0.144	110.5	18.0
Sharp SLM-notch (SLM-N)	110	60375	0.514	116.3	15.2
Blunt turned-notch (T-N)	102	3782	0.313	116.6	11.8
Blunt SLM-notch (SLM-N)	83	715	0.138	148.8	17.2

Table 2. Size of the critical defects found from fractographic analyses done on 3 specimens per experimental batch.

Specimen geometry	Critical defect size $\sqrt{area}_{\max}$ (µm)		
	Min	Max	Mean
Plain	107	226	158
Sharp turned-notch (T-N)	220	228	223
Blunt turned-notch (T-N)	135	292	216
Sharp SLM-notch (SLM-N)	44	88	63
Blunt SLM-notch (SLM-N)	46	95	65

Table 3. Scenarios envisaged for the calibration of the threshold fatigue model expressed by Eq. (11).

Scenario	Dataset
S1	Sharp SLM-N + Sharp T-N + Plain
S2	Sharp SLM-N + Blunt SLM-N + Plain
S3	Sharp T-N + Blunt T-N + Plain
S4	Blunt SLM-N + Blunt T-N + Plain

Table 4. Best-fit parameters of the threshold fatigue model expressed by Eq. (11).

Scenario	ΔK_{th} (MPa m$^{0.5}$)	a_0 (mm)	$\Delta\sigma_0/2$ (MPa)
S1	7.31	0.01441	543.3
S2	7.49	0.02518	420.9
S3	7.19	0.01831	473.7
S4	7.48	0.03138	376.7

Table 5. Prediction of the high-cycle fatigue strength (N_f=5×10^7 cycles) for the five experimental variants considered in this work.

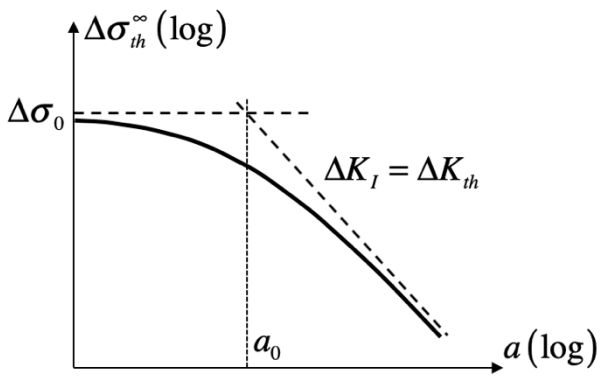| Condition	Exp. (MPa)	Scenario							
		S1		S2		S3		S4	
		Pred. (MPa)	Err. (%)	Pred. (MPa)	Err. (%)	Pred. (MPa)	Err. (%)	Pred. (MPa)	Err. (%)
Sharp SLM-N	116.3	114.6	-1.5	104.5	-10.1	107.6	-7.5	98.6	-15.2
Sharp T-N	110.5	102.0	-7.7	99.7	-9.8	98.5	-10.9	97.1	-12.1
Blunt SLM-N	148.8	174.2	17.1	159.2	7.0	163.8	10.1	150.4	1.1
Blunt T-N	116.6	125.5	7.6	122.4	5.0	121.1	3.9	119.2	2.2
Plain	225.0	233.8	3.9	224.4	-0.3	224.3	-0.3	216.8	-3.6
Error r.m.s. (%)		9.2		7.4		7.6		8.9	

Figures

Figure 1. Schematic representation of the Kitagawa-Takahashi diagram.
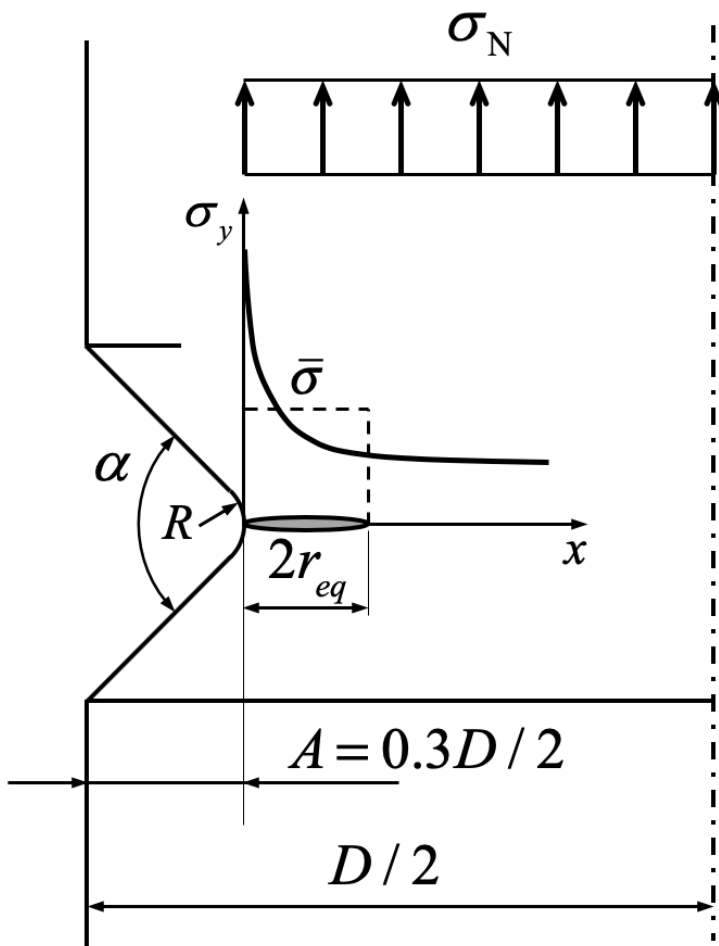

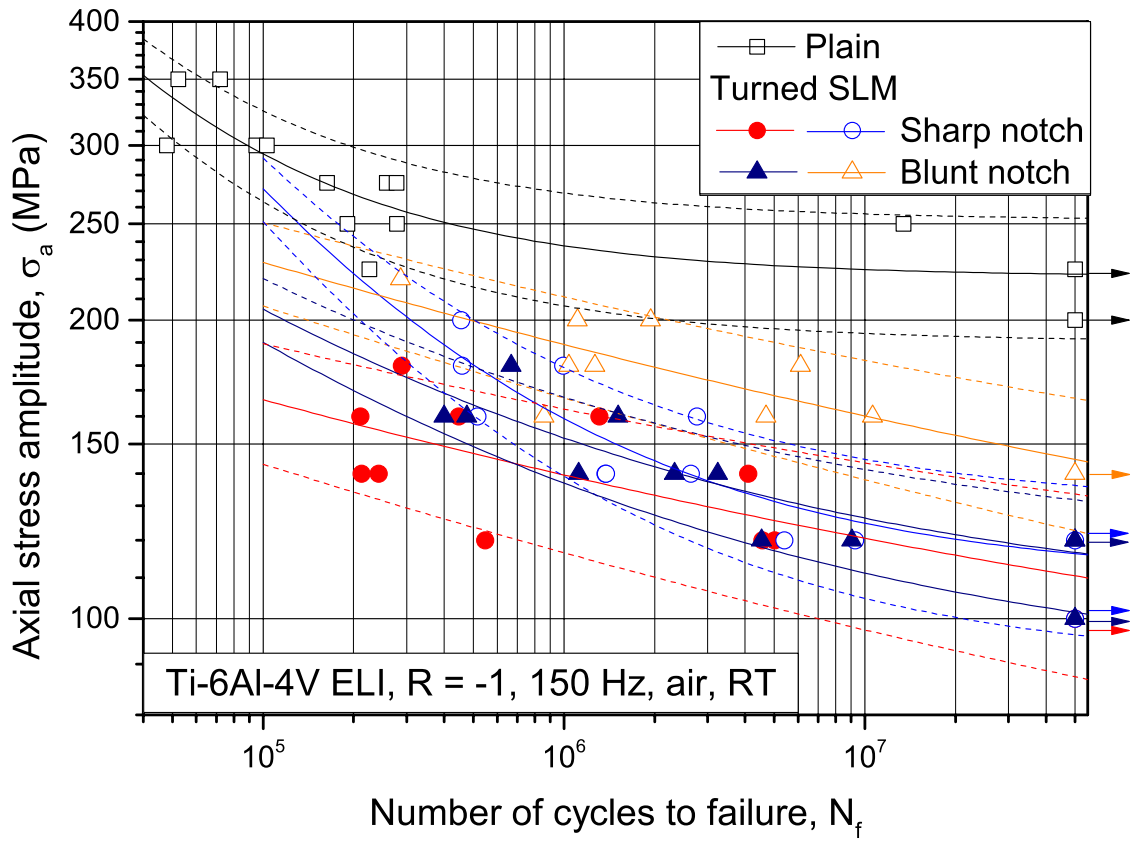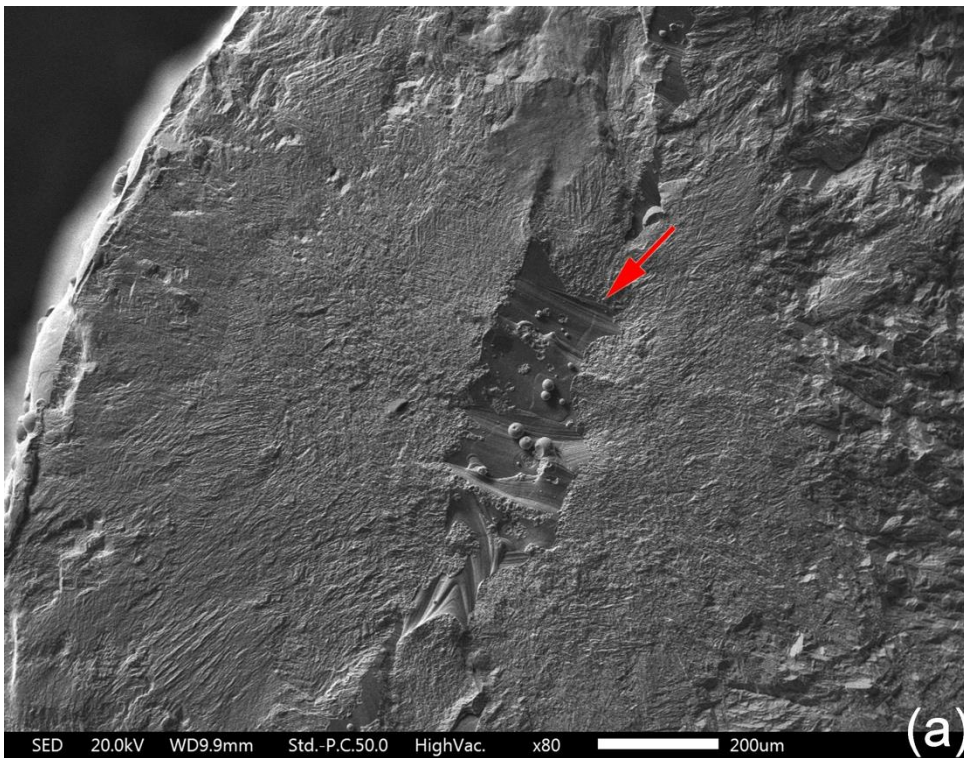Figure 2. Geometry of the optimized V-notched cylindrical specimen.

Figure 3. Axial fatigue SN curves. Solid lines represent 50% failure probability, while dashed lines refer to 10% and 90% failure probability.
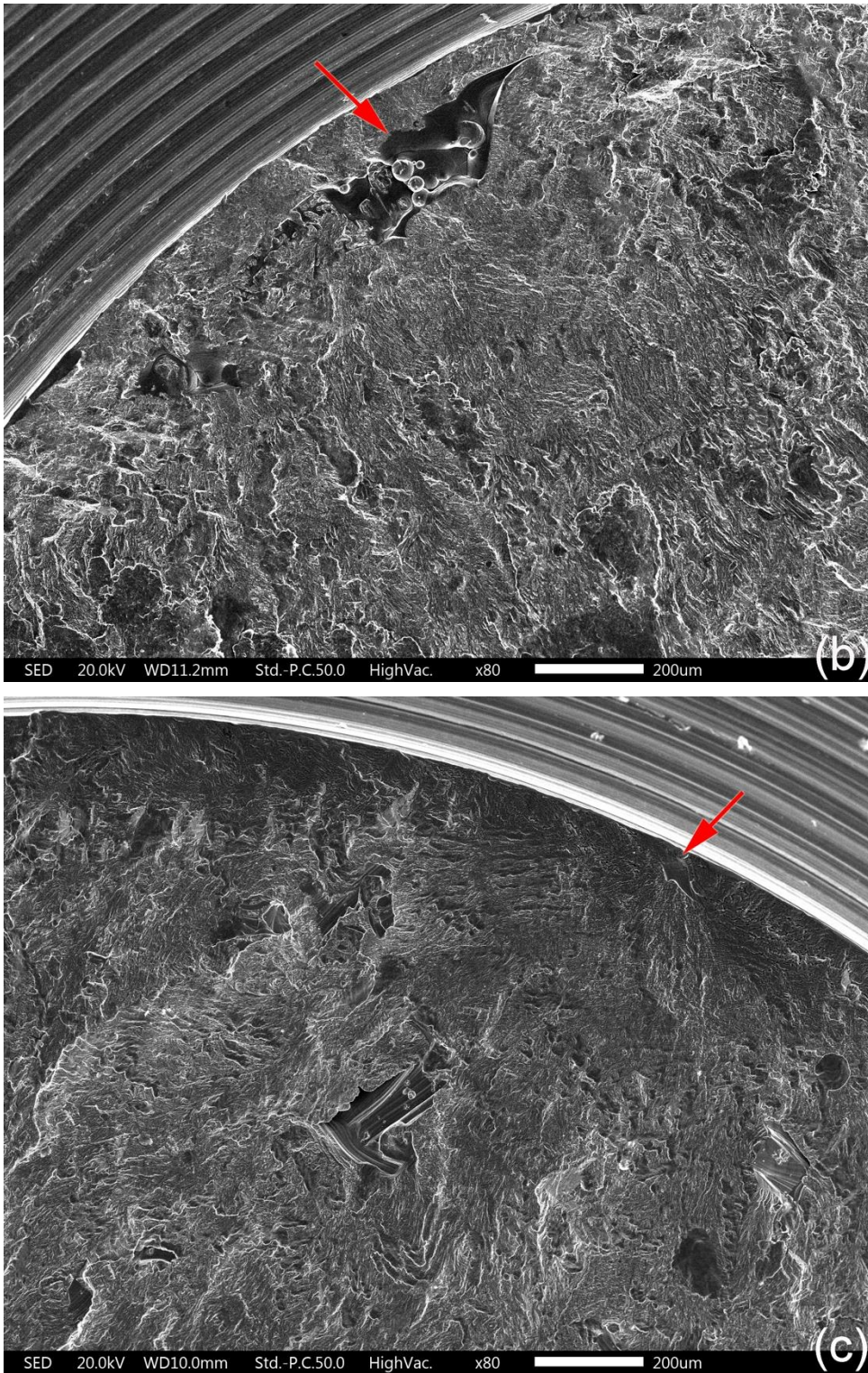
Figure 4. SEM micrographs of the fracture surfaces around the fatigue crack initiation site. (a) plain sample (σ_a = 250 MPa, N_f=1.3×10^7 cycles), (b) sharp turned notched (T-N) sample (σ_a = 120 MPa, N_f=4.6×10^6 cycles), (c) sharp SLM notched (SLM-N) sample (σ_a = 140 MPa, N_f=2.6×10^6 cycles). The critical defect is marked by a red arrow.
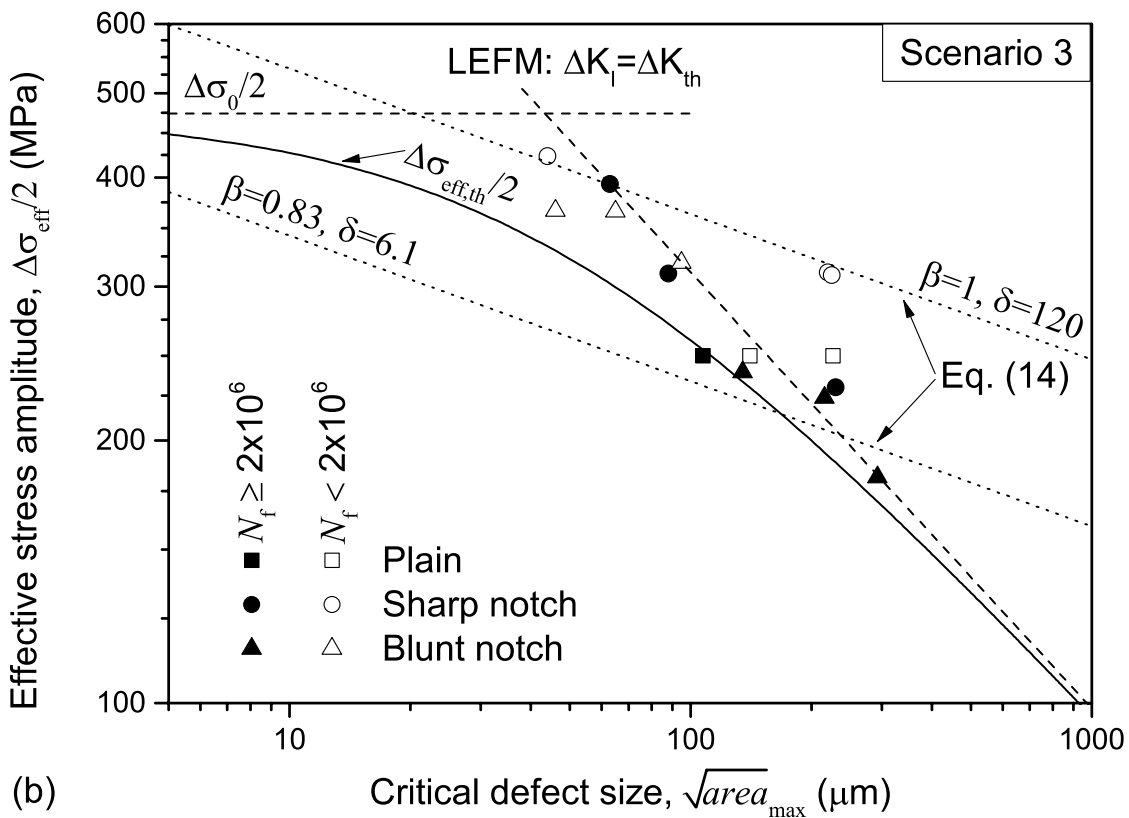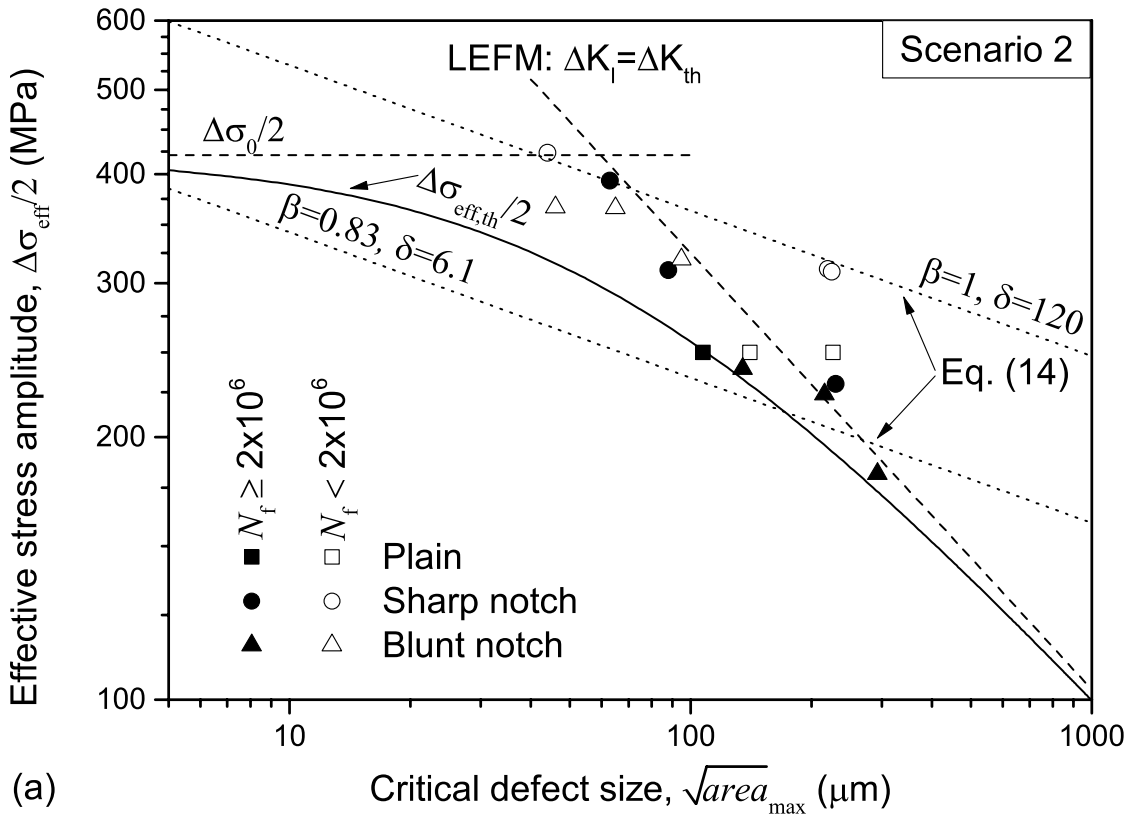
Figure 5. Kitagawa-Takahashi diagram of the alloy Ti-6Al-4V ELI additively manufactured via SLM plotted as a function of the critical defect size. The parameters of the model have been inversely determined from the fatigue data of the scenario 2 (a) and 3 (b) listed in Table 3. The close (open) symbols refer to results of fatigue tests ended after (before) 2 million cycles.